

Dynamic and polarization-independent high-*Q* guided resonances in metasurfaces with phase change material

Guozhong Zhang(张国忠), Mimi Zhou(周秘密), Hong Xiang(向红), and Dezhuan Han(韩德专),
Citation: Chin. Phys. B, 2025, 34 (**8**): 084201. DOI: 10.1088/1674-1056/add1bb
http://cpb.iphy.ac.cn; http://iopscience.iop.org/cpb

What follows is a list of articles you may be interested in

Giant-tunable bidirectional Goos-Hänchen shifts via phase change material-based metasurfaces with quasi-bound states in continuum

Jiaqing Liu(刘佳晴), Yue Zheng(郑悦), Xiao Li(李潇), Jingwen Li(李静文), Guohao Zhang(张国昊), Daxing Dong(董大兴), Dongmei Liu(刘冬梅), Yuwen Jia(贾玉雯), Yangyang Fu(伏洋洋), and Youwen Liu(刘友文)
Chin. Phys. B, 2025, 34 (**7**): 074208. DOI: 10.1088/1674-1056/adcdee

Symmetry-protected and Brillouin zone folding driven bound states in the continuum in dielectric nanorod arrays for efficient third harmonic generation

Wen-Jing Wang(王文静), Shi-Jie Liang(梁世杰), Jia-Qi Zou(邹家祺), Yan-Yan Huo(霍燕燕), and Ting-Yin Ning(宁廷银)
Chin. Phys. B, 2025, 34 (**3**): 034202. DOI: 10.1088/1674-1056/ada2f0

Active control of surface plasmon polaritons with phase change materials

Yuan-Zhen Qi(漆元臻), Qiao Jiang(蒋瞧), Hong Xiang(向红), and De-Zhuan Han(韩德专)
Chin. Phys. B, 2023, 32 (**10**): 104202. DOI: 10.1088/1674-1056/accd5a

Temperature-responded tunable metalenses based on phase transition materials

Jing-Jun Wu(伍景军), Feng Tang(唐烽), Jun Ma(马骏), Bing Han(韩冰), Cong Wei(魏聪), Qing-Zhi Li(李青芝), Jun Chen(陈骏), Ning Zhang(张宁), Xin Ye(叶鑫), Wan-Guo Zheng(郑万国)‡, and Ri-Hong Zhu(朱日宏)
Chin. Phys. B, 2022, 31 (**5**): 054216. DOI: 10.1088/1674-1056/ac3cad

Thermal tunable one-dimensional photonic crystals containing phase change material

Yuanlin Jia(贾渊琳), Peiwen Ren(任佩雯), and Chunzhen Fan(范春珍)†
Chin. Phys. B, 2020, 29 (**10**): 104210. DOI: 10.1088/1674-1056/abab78

Dynamic and polarization-independent high-Q guided resonances in metasurfaces with phase change material

Guozhong Zhang(张国忠), Mimi Zhou(周秘密), Hong Xiang(向红)[†], and Dezhuan Han(韩德专)[‡]

Department of Physics and Chongqing Key Laboratory for Strongly Coupled Physics, Chongqing University, Chongqing 401331, *China*

(Received 12 February 2025; revised manuscript received 22 April 2025; accepted manuscript online 29 April 2025)

Using periodic refractive index perturbations, the Brillouin zone is folded, transforming the guided modes in a metasurface into guided resonances with arbitrarily high quality-factors. The incorporation of phase change materials within the metasurface enables dynamic modulation of the guided modes. The system's symmetry ensures a polarization-independent response under normal incidence. Furthermore, the metasurface exhibits excellent sensing performance, demonstrating its potential for advanced photonic applications.

Keywords: Brillouin zone folding, phase change material, guided resonance, sensing

PACS: 42.25.Bs, 42.25.Ja, 78.67.Pt, 78.20.N–

DOI: 10.1088/1674-1056/add1bb **CSTR:** 32038.14.CPB.add1bb

1. Introduction

To enhance light–matter interactions at the nanoscale, resonances with high quality (Q) factors are crucial. Periodic structures such as resonant waveguide gratings,[1–3] photonic crystal slabs,[4–7] and metasurfaces[8,9] can serve as free-space-accessible platforms for high-Q resonances. In dielectric metasurfaces with periodic structures, three typical modes are supported: guided modes (GMs), Fabry–Parot modes, and the guided resonances (GRs).[4] GMs are inaccessible from free space while Fabry–Parot modes exhibit very low Q factors. Consequently, GRs are commonly exploited to achieve high Q resonances.

A theoretically infinite high Q factor for GRs can be achieved through the construction of bound states in the continuum (BICs).[5,10] BICs are a special class of GRs that are typically discretely distributed on GR bands. These states arise from the incompatible symmetries of the GR and the corresponding free space modes (symmetry-protected BICs), or the destructive interference of the radiative components in the GRs (Friedrich–Wintgen BICs). By definition, BICs are fully decoupled from the free space radiation and thus are inaccessible for most situations. Designing a BIC with specific frequency and momentum requires precise parameters tuning. When these parameters deviate from their ideal values, a BIC transitions into an accessible quasi-BIC with a finite yet very high Q factor.[5,11,12] However, the Q-factor of a quasi-BIC is very sensitive to parameter variations, requiring careful design for devices based on quasi-BICs. Furthermore, quasi-BICs induced by symmetry breaking often exhibit polarization anisotropy, which may limit their stability in applications such as sensing.

Beyond BICs, non-BIC GRs also offer a viable pathway for achieving high-Q resonances. A straightforward yet effective approach involves folding the Brillouin zone by introducing periodic perturbations to the lattice.[1,13,14] This process reduces the Brillouin zone, by half, for example, folding the guided modes into the region of continuum to form GRs. As these GRs originate from guided modes, they inherit inherently high Q factors. Furthermore, the Q factors can be readily tuned by the strength of the perturbations.[3,15] By this means, GRs with Q-factor as high as 2.4×10^5 have been experimentally realized.[16] Unlike quasi-BICs, these GRs do not rely on symmetry breaking, enabling the possibility of polarization-independent excitation. Additionally, such GRs are insensitive to the angle of incident light,[14] which enhances the stability and reliability of associated devices.

The optical properties of a device are typically determined by its structural design. However, dynamic tuning of metasurfaces is highly desirable for many applications. Various approaches have been proposed to enable dynamic modulation in metasurfaces. In the terahertz band, dynamic resonances have been demonstrated in dielectric silicon metasurfaces by modifying the material carrier density through photo-doping, achieved by applying a short-pulse optical pump with photon energy greater than the silicon band gap.[17,18] Similarly dynamic graphene–dielectric composite metasurfaces have been realized using the electro-doping to modulate graphene conductivity, where voltage adjustments alter the Fermi energy.[10,15,19] In the near-infrared (NIR) band, dynamic quasi-BICs have been achieved using photosensitive material based metasurface[20] and nanoelectromechani-

[†]Corresponding author. E-mail: xhong@cqu.edu.cn

[‡]Corresponding author. E-mail: dzhan@cqu.edu.cn

© 2025 Chinese Physical Society and IOP Publishing Ltd. All rights, including for text and data mining, AI training, and similar technologies, are reserved.

cal systems.[21] In addition, phase change materials (PCMs) have emerged as promising candidates for dynamic modulation in micro- and nano-photonic systems. PCMs demonstrate excellent performance[22–25] due to their ability to reversibly modulate crystallinity via optical, thermal, or electrical methods, coupled with fast response time, high stability and significant refractive index contrast.[26,27] Among these PCMs, Sb_2S_3[28] and Sb_2Se_3[14,29] exhibit substantial refractive index differences between their amorphous and crystalline states while maintaining low optical losses in both states within the NIR regime.

Despite their potential, studies on dynamic guided resonances (GRs) in the NIR band using low-loss PCMs remain limited, particularly for high-Q GRs achieved through Brillouin zone folding. Exploring the use of PCMs to modulate periodic perturbations in metasurfaces offers a novel and promising avenue for advancing dynamic, high-Q optical resonances.

In this paper, we propose a dielectric metasurface composed of Sb_2Se_3 (SS) to achieve dynamic high-Q resonances in the NIR band. The metasurface supports polarization independent dual-band high-Q GRs through band folding induced by periodic refractive index perturbations. These GRs are demonstrated to be insensitive to the wavevector and polarization of the incident light. The optical response of the metasurface is modulated flexibly by tuning the refractive index of the PCM. We further demonstrate the utility of these GRs in refractive index sensing, investigating how their tunability enhances and modulates the figure of merit (FoM). To address challenges associated with the crystallinity control, we also present alternative approaches for realizing tunable GRs. Our findings expand the possibilities for implementing of polarization-independent and dynamically tunable GRs, offering significant potential for high-Q optical resonances and advanced photonic applications.

2. Results and discussion

2.1. Perturbation scheme and band structures of the metasurface

As shown in Fig. 1(a), the proposed metasurface is formed by periodically arranging the SS discs on an SiO_2 substrate. When no phase transition occurs, the 4 discs labeled A, B, C, D in a super cell are identical. Experimentally, the metasurface can be obtained by depositing an SS layer with a uniform thickness onto a glass substrate, followed by the processing of electron-beam lithography (EBL) and inductively coupled plasma (ICP) etching techniques. The radius R and thickness h of the SS nanodiscs are set as 200 nm and 220 nm, respectively. The distance between the two nearest nanodiscs is $d = 500$ nm. The optical properties of the metasurface were evaluated using the finite element method (FEM). Periodic boundary conditions are applied in the x and y directions, and perfectly matched layers are set in the z direction. The refractive index of SiO_2 in the near-infrared wavelengths is adopted from the experimental data of Palik.[30] The refractive indices and extinction coefficients of SS are extracted from the reported experimental data.[31] Two types of refractive index perturbation are proposed for the metasurface, as illustrated in Fig. 1(b). In the first scenario, the four discs are initially in an amorphous state, with disc A gradually transitioning into a crystalline state. Conversely, in the second scenario, the discs are initially in a crystalline state, and disc A gradually transitions into an amorphous state.

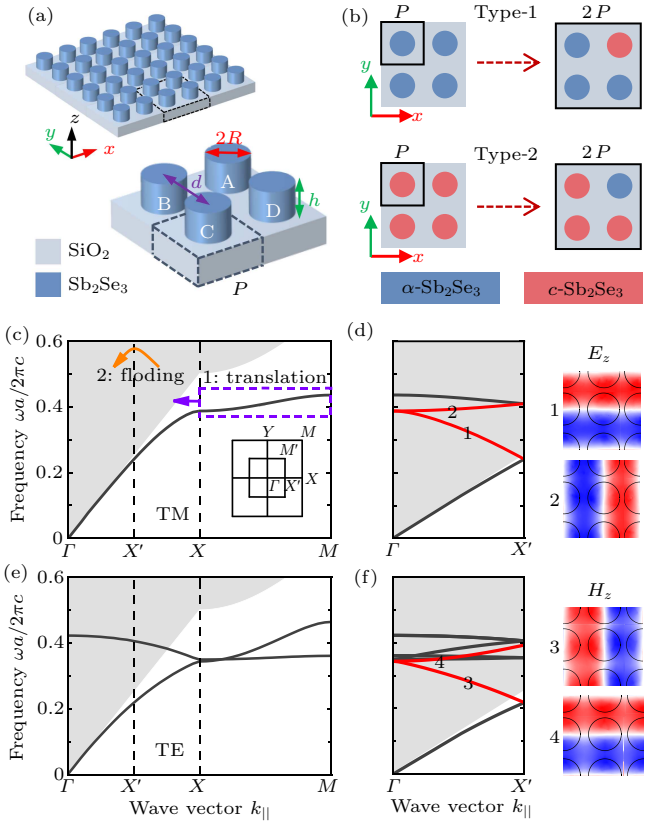


Fig. 1. (a) Schematic diagram of the proposed metasurface. (b) Two types of perturbations of the refractive index. Type-1: the four discs are all initially in an amorphous state, followed by the transformation of nanodisc A into a crystalline state. Type-2: all four discs are initially in a crystalline state, followed by the transformation of nanodisc A into an amorphous state. (c)–(f) Illustration of the band structures of the TM (TE) modes before and after the perturbation. The insets next to panels (d) and (f) are the field profiles for bands 1–4 at the Γ point.

When there is no perturbation, each unit cell of the metasurface contains only one disc and the period $P = 500$ nm. The transverse electric (TE) and transverse magnetic (TM) band structures in the first Brillouin zone along Γ–X–M direction were calculated, as shown in Figs. 1(c) and 1(e), respectively. Note here no substrate is considered for simplicity. The lowest band lies outside of the light cone (gray shaded region), corresponding to the non-radiative guided modes. When perturbation described above is introduced, the unit cell expands

to four times its original size and hence, the Brillouin zone will be compressed to 1/4 of its original area.[32] The corresponding band structure can be obtained from successive Brillouin zone folding along the k_x and k_y directions. Such operation will map the original high-symmetry points X, Y, and M point onto the Γ point. As a result, a single band in the original Brillouin zone transforms into four distinct bands. Specifically, the band structure along the k_x direction consists of four branches, corresponding to the original Γ–X', X'–X, Y–Y', and M–Y' segments. Owing to the C_4 rotational symmetry of the lattice, the dispersion along the Y–M segment is equivalent to that of the X–M segment. Therefore, the band structure along the k_x direction can be constructed following the procedure illustrated in Fig. 1(c): (i) translate the X–M segment to the Γ–X segment, doubling the number of bands in this region; (ii) fold the resulting band structure in the Γ–X segment in the k_x direction. The final folded band structures are presented in Figs. 2(d) and 2(f).

The field profiles corresponding to the bands at the Γ point are calculated. Insets in Figs. 1(d) and 1(f) illustrate the field distributions (E_z for TM modes and H_z for TE modes) of the degenerate bands (labeled as 1, 2 for the TM modes and 3, 4 for the TE modes). These profiles are centered on nanodisc A, which serves as the symmetry center of the perturbed system. The results reveal that the profiles exhibit C_2-odd symmetry and the degenerate pairs are connected by a 90° rotation. Conversely, other field profiles (not shown here) demonstrate C_2-even symmetry. The distinction in symmetry imply that C_2-odd modes can be excited by far-field radiation, whereas the C_2-even modes cannot, giving rise to the symmetry-protected BICs.[10]

2.2. Dynamic tuning of metasurface transmission

Figure 2 shows the transmission spectra of the metasurfaces at normal incidence under the refractive index perturbations by manipulating the crystallinity of nanodisc A (m_A). Figures 2(a) and 2(b) correspond to type-1 and type-2 perturbations, respectively. When no perturbation is applied, no resonance peak is observed in the frequency regime of interest. In this case, no band folding happens and all the modes concerned resides below the light line and are GMs, as indicated by Figs. 1(c) and 1(e). When period perturbations are introduced, the transmission spectra show that 2 resonances are excited. For convenience, these resonances are labeled as modes I, II, I′, and II′, respectively. By the field profiles, the two modes excited can be recognized as the two degenerate pairs shown in Figs. 1(d) and 1(f). Modes I and I′ come from the TM bands 1 or 2; modes II and II′ come from the TE bands 3 or 4. When incident light is x-polarized, the Γ point modes on band 1 of the TM, band 4 of the TE bands will be excited. While for y-polarized incidence, band 2 of the TM and band 3 of the TE bands will be excited.

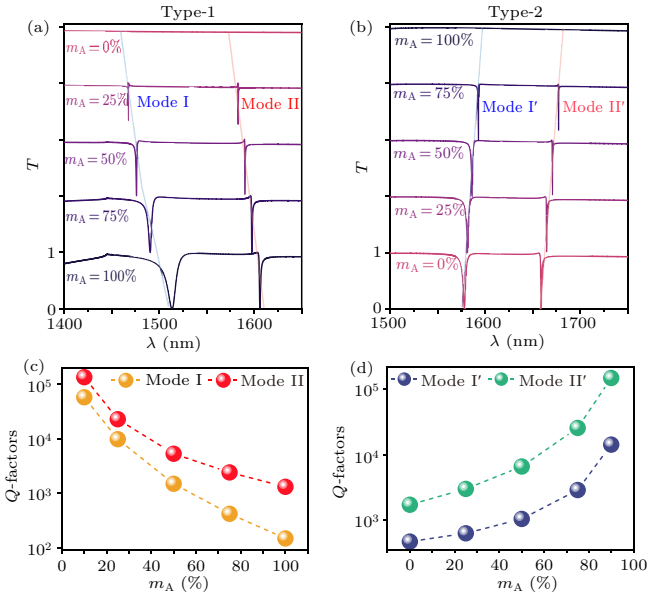


Fig. 2. (a) and (b) Transmission spectra of the metasurfaces corresponding to perturbation of the type-1 and type-2 shown in Fig. 1(b) with different crystallinities. (c) and (d) Q-factors of the modes shown in panels (a) and (b). Here m_A is the crystallinity of the SS nanodisc A.

The Q-factors and the resonant frequencies can be modulated readily by the strength of perturbation. As shown in Figs. 2(c) and 2(d), with the increase of the perturbation via crystallinity modulation, the width of the resonance peak increases and the resonance frequencies shift to the blue side or red side, depending on change of the effective refractive index arising from the crystallinity variation.

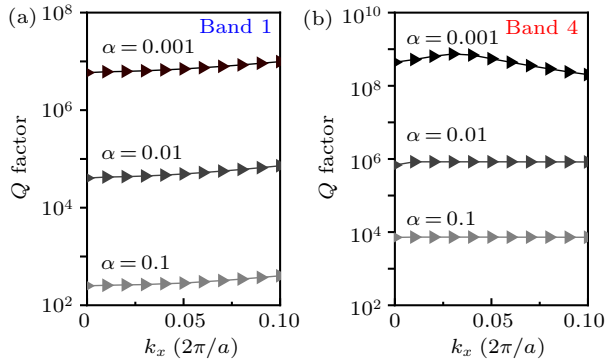


Fig. 3. The Q-factors of GR modes of band 1 (a) and band 4 (b) in momentum space with different perturbation factors.

Different from the quasi-BICs, the Q-factors of GRs are insensitive to the variation of the wave vector.[14] Figure 3 shows the Q-factors of the two GRs at the vicinity of the Γ point under different perturbations. Here the perturbation factor is defined as $\alpha = (n_A n_{other})/n_{other}$, where n_A denotes the refractive index of nanodisc A, and n_{other} represents the refractive index of the other three nanodiscs in the unit cell. The refractive index of the substrate remains constant throughout the

analysis. Unlike the quadratic momentum dependence ($\propto k^{-2}$) of the quasi-BICs,[33–36] the Q–k_x relation of the GRs exhibit a flat feature, consistent with the previous report.[14] Such insensitivity might be favorable for the stability of associated devices.

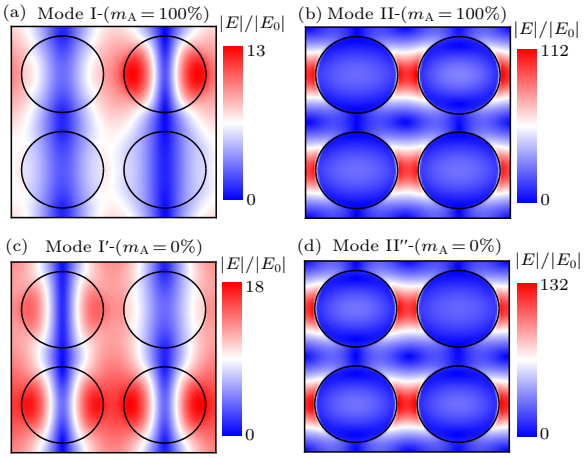


Fig. 4. Electric field distributions of the guided resonances at normal incidence. Panels (a) and (b) correspond to type-1 perturbation while panels (c) and (d) correspond to type-2 perturbation.

Figure 4 shows the electric field distributions in the x–y plane at the midplane of the nanodiscs for the four resonances under maximum perturbation. Comparing modes I and I′ with modes II and II′ reveals two key differences. First, the sensitivity of the field distributions to perturbation differs significantly. In modes I and I′, the field distribution at nanodisc A differs considerably from that of the other nanodiscs, whereas in modes II and II′, this difference is much smaller. This variation accounts for the differences in their Q-factors, since a more pronounced difference in field distribution indicates a greater deviation from the waveguide mode, resulting in a lower quality factor. Second, compared to modes I and I′, the electric fields in modes II and II′ are more concentrated in the gap between the nanodiscs, with a much stronger relative electric field strength $|E|/|E_0|$ (where E and E_0 denote the local electric field and the incident electric field, respectively). This distinction suggests that modes II and II′ are more suitable for sensing applications.

2.3. Polarization-independence of the metasurface

Achieving polarization-independent optical cavities, i.e., the resonances remain stable under polarization changes, is important for many applications. For the index perturbation proposed here, the C_4 symmetry can be remained naturally. Figure 5(a) shows the planar schematic diagram of the metasurface in which the red discs (denoted as A) are perturbed. Though no C_4 symmetry can be directly seen from the supercell indicated by the black solid box. However, if we choose the red discs or their diagonal neighbours as the center of the supercell, as indicated by the red or yellow box, it is obvious that the metasurfaces maintain the C_4 symmetry. Such symmetry ensures that the metasurface is isotropic to polarization for normal incidence.[37] Figures 5(c) and 5(d) show the transmission of the metasurface with different polarization angel θ, it can be seen that the locations and intensities of the GRs are independent of the polarization.

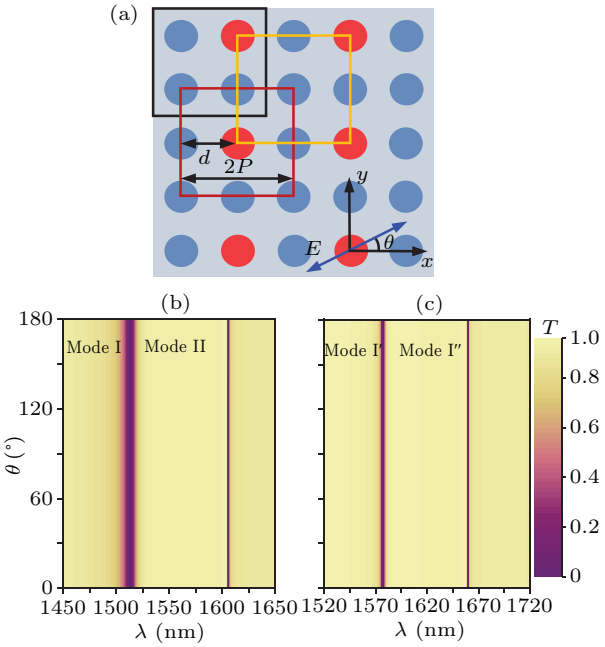


Fig. 5. (a) Schematic diagram of the supercells. The unit cells indicated by the yellow or red box show that the lattice possesses C_4 symmetry. Nanodiscs with the same crystallinity are shown in the same color. The inset describes the polarization of the normal incidence. (b) Transmission at different polarization angles under type-1 perturbation with $m_A = 100\%$. (c) Transmission at different polarization angles under type-2 perturbation with $m_A = 0\%$.

The polarization independence is related to the mode degeneracy at the Γ point. As shown in Fig. 1, the field profiles of the degenerate modes (band 1 and band 2 in the TM bands, band 3 and band 4 in the TE bands.) are the same up to a 90° rotation. At normal incidence, the Γ point modes on band 1 (2) of the TE polarization, band 4 (3) of the TM polarization are excited when light is $x(y)$-polarized. For incidence with arbitrary polarization angle, both modes will be excited. However, since the field profiles are essentially identical, the spectra remain unchanged, ensuring polarization independence.

It worth noting that this polarization independence is valid only under normal incidence. At oblique incidence, the overall C_4 symmetry of the system (with the incidence included) is broken, thereby eliminating the polarization invariance. As a result, the corresponding bands are excited by the x- or y-polarized components of the incident field. Due to their distinct dispersion properties, shift and splitting of the resonant peaks will be observed.

2.4. Sensing applications of the metasurface

As high Q-factor resonances, GRs supported in the dielectric metasurface can facilitate the sensing applications by

affording exceptional near-field enhancement. The sensing capabilities are often evaluated by two metrics: sensitivity ($S = \Delta\lambda/\Delta n$) and the figure of merit (FoM = S/FWHM). Here $\Delta\lambda$ denotes the shift of the resonance peak, Δn signifies the variation of the refractive index of the analyte, and FWHM is the full width at half maximum of the resonance peak. Here we provide an illustrative example of ambient refractive index sensing. The metasurface is situated within ambient media characterized by varying refractive indices. With the transmission spectra corresponding to distinct levels of crystallinity variation under both type-1 and type-2 perturbations obtained, the sensing performance can be evaluated.

The positions of the resonance peaks for type-1 and type-2 perturbations are plotted respectively in Figs. 6(a) and 6(c) as a function of the ambient refractive index, and the corresponding FoMs are depicted in Figs. 6(b) and 6(d). According to the definition, the sensitivity S is given by the slope of curves plotted in Figs. 6(a) and 6(c). According to Fig. 6(a), the sensitivity is about 200 nm/RIU (RIU: refractive index unit) for mode I and 600 nm/RIU for mode II under type-1 perturbation. Likewise, under type-2 perturbation, mode I′ showcases a sensitivity of 200 nm/RIU while mode II′ displays a sensitivity of 660 nm/RIU (see Fig. 6(c)). The long wavelength modes consistently exhibit higher sensitivity compared to their short wavelength counterparts. This sensitivity distinction can be attributed to the different field profiles illustrated in Fig. 4. Comparing to modes I and I′, the electric fields associated with modes II and II′ are more concentrated within the gap between the nanodiscs, thereby engendering more pronounced field-analyte interactions.

Within the discussed ambient refractive index range, modulation and enhancement of the FoM values are achieved, while the sensitivity remains virtually unaffected by m_A. In Figs. 6(b) and 6(d), the FoMs of the resonant modes corresponding to Figs. 6(a) and 6(c) are presented. It can be observed that the FoM exhibits minimal dependence on the ambient refractive index. On the other hand, due to the larger FWHM (lower Q-factor) and lower sensitivity, the short-wavelength modes exhibit lower FoM values compared to the long-wavelength modes. The FoM can be tuned by controlling the crystallinity of nanodisc A. Compared to recently reported sensors operating in the infrared region,[2,31,38–42] the proposed sensor demonstrates excellent performance in terms of sensitivity, quality factor, polarization insensitivity, and dynamic tunability.

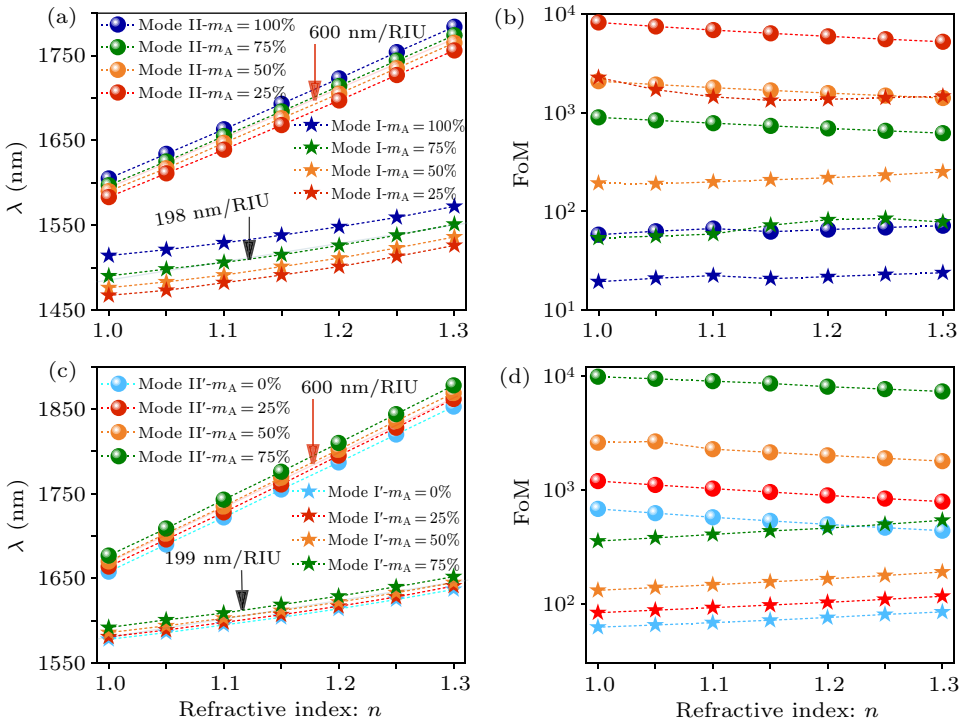


Fig. 6. The wavelengths of the resonance peaks and the corresponding FoMs as a function of the ambient refractive index. Panels (a) and (b) are for the type-1 perturbation, while panels (c) and (d) are for the type-2 perturbation.

2.5. Simplified version of the tunable metasurface

Precise control of the partial crystallization of PCMs remains a significant challenge in practice, whereas transitioning between the amorphous and crystalline states is relatively straightforward. Additionally, comparing to modulate the crystallinity of specific nanodiscs within a metasurface, controlling the crystallinity of the entire metasurface is considerably more feasible. To address this, we adopt a simplified strategy to design a tunable metasurface that relies exclusively

on the amorphous and crystalline states.

As illustrated in Fig. 7(a), the refractive index perturbation is implemented by modifying the size of nanodisc A, with dynamic control achieved through transitions between the amorphous and crystalline states. This structure exhibits a similar band structure to that in Fig. 1 and supports two pairs of degenerate guided resonance (GR) modes at the Γ-point. The system retains C_4 symmetry, ensuring polarization-independent optical responses.

The transmission spectra of the metasurface corresponding to the two crystallinity states are shown in Fig. 7(b). Two resonance modes are observed, designated as mode I (short wavelength) and mode II (long wavelength), with their corresponding Q factors presented in Fig. 7(c). Here the radius of the disc on top left is reduced from 200 nm to 185 nm, enabling the Q-factors to be tuned between 10^3 and 10^4. Notably, smaller radius reduction can yield higher Q-factors. Under realistic fabrication conditions, the Q factors are significantly reduced due to fabrication imperfections. Nevertheless, simulation results suggest that Q factors on the order of several hundred can still be achieved if variations in nanodisc diameter are constrained to approximately ± 10 nm, which remains adequate for many practical applications.

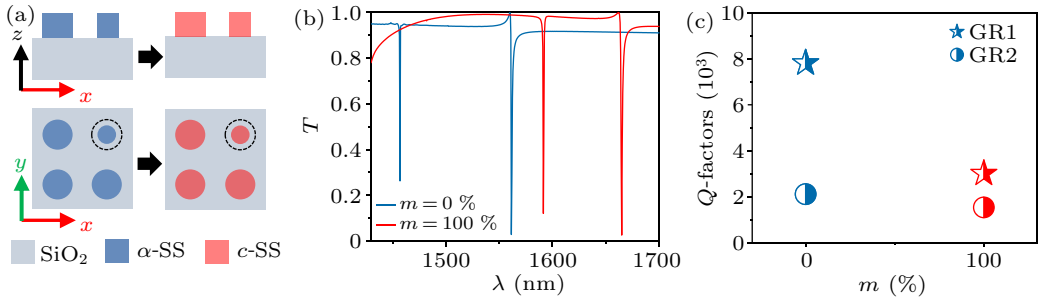


Fig. 7. (a) Side view (top) and top view (bottom) of the unit cell of the size-perturbed metasurface. The black arrows indicate the transition from the amorphous state to crystalline state. The transmission spectra and the corresponding Q-factors of the metasurface in the crystalline and amorphous states are shown in panels (b) and (c).

3. Conclusion

In conclusion, we propose a refractive index-tunable and low-loss metasurface based on the phase change material. The excitation and dynamic modulation of the polarization-independent GRs are achieved by manipulating the crystallinity of the phase change material. As the GRs arise from the band folding which turns the GMs into GRs, their Q-factors can be straightforwardly modulated by the extent of perturbation and exhibit a good tolerance to the angle of incidence. Meanwhile, due to the C_4 symmetry of the system, the transmission spectra are independent of the incidence polarization.

As an example of application, the sensing performance of the tunable metasurface is evaluated. The sensitivities of the two dual-band GRs were near 200 nm/RIU and 600 nm/RIU, respectively. Meanwhile the corresponding FoM can be modulated effectively from tens to thousands by means of crystallinity tuning. We also propose a more experimentally convenient scheme to achieve tunable and polarization-independent GRs with high Q factors.

Our work provides a promising pathway to achieve tunable polarization-independent high-Q modes and may facilitates related applications.

Acknowledgement

Project supported by the National Natural Science Foundation of China (Grant No. 12347101).

References

[1] Overvig A C, Shrestha S and Yu N 2018 *Nanophotonics* **7** 1157
[2] Liu C, Bai Y, Zhou J, Chen J and Qiao L 2021 *Opt. Express* **29** 42978
[3] Shi W, Gu J, Zhang X, Xu Q, Han J, Yang Q, Cong L and Zhang W 2022 *Photonics Research* **10** 810
[4] Fan S and Joannopoulos J D 2002 *Phys. Rev. B* **65** 235112
[5] Yin X, Jin J, Soljačić M, Peng C and Zhen B 2020 *Nature* **580** 467
[6] Jin J, Yin X, Ni L, Soljačić M, Zhen B and Peng C 2019 *Nature* **574** 501
[7] Zhang Z, Qin F, Xu Y, Fu S, Wang Y and Qin Y 2021 *Photonics Research* **9** 1592
[8] Liu Z, Xu Y, Lin Y, Xiang J, Feng T, Cao Q, Li J, Lan S and Liu J 2019 *Phys. Rev. Lett.* **123** 253901
[9] Jia S, Li Y, Xue Z, Chen K, Li Z, Gong Q and Chen J 2023 *Adv. Mater.* **35** 2212244
[10] Gao E, Jin R, Fu Z, Cao G, Deng Y, Chen J, Li G, Chen X and Li H 2023 *Photonics Research* **11** 456
[11] Koshelev K, Lepeshov S, Liu M, Bogdanov A and Kivshar Y 2018 *Phys. Rev. Lett.* **121** 193903
[12] Li S, Zhou C, Liu T and Xiao S 2019 *Phys. Rev. A* **100** 063803
[13] Zeng B, Majumdar A and Wang F 2015 *Opt. Express* **23** 12478
[14] Wang W, Srivastava Y K, Tan T C, Wang Z and Singh R 2023 *Nat. Commun.* **14** 2811
[15] Chen Y, Liu Z, Li Y, Hu Z, Wu J and Wang J 2022 *Opt. Express* **30** 23828
[16] Huang L, Jin R, Zhou C, Li G, Xu L, Overvig A, Deng F, Chen X, Lu W, Alù A and Miroshnichenko A E 2023 *Nat. Commun.* **14** 3433
[17] Fan K, Shadrivov I V and Padilla W J 2019 *Optica* **6** 169
[18] Han S, Cong L, Srivastava Y K, Qiang B, Rybin M V, Kumar A, Jain R, Lim W X, Achanta V G, Prabhu S S, Wang Q J, Kivshar Y S and Singh R 2019 *Adv. Mater.* **31** 1901921
[19] Li J, Li J, Zheng C, Yue Z, Wang S, Li M, Zhao H, Zhang Y and Yao J 2021 *Carbon* **182** 506
[20] Mikheeva E, Koshelev K, Choi D Y, Kruk S, Lumeau J, Abdeddaim R, Voznyuk I, Enoch S and Kivshar Y 2019 *Opt. Express* **27** 33847
[21] Kwon H, Zheng T and Faraon A 2021 *Nano Lett.* **21** 2817
[22] Dong W, Liu H, Behera J K, Lu L, Ng R J, Sreekanth K V, Zhou X, Yang J K and Simpson R E 2019 *Adv. Funct. Mater.* **29** 1806181
[23] Zhou C, Qu X, Xiao S and Fan M 2020 *Phys. Rev. Appl.* **14** 044009

[24] Zhang Y, Fowler C, Liang J, Azhar B, Shalaginov M Y, Deckoff-Jones S, An S, Chou J B, Roberts C M, Liberman V, Kang M, Ríos C, Richardson K A, Rivero-Baleine C, Gu T, Zhang H and Hu J 2021 *Nat. Nanotechnol.* **16** 661
[25] Zhuo S, Li Y, Zhao A, Li Y R, Yao S, Zhang M, Feng T and Li Z 2023 *Laser & Photon. Rev.* **17** 2200403
[26] Abdollahramezani S, Hemmatyar O, Taghinejad H, Krasnok A, Kiarashinejad Y, Zandehshahvar M, Alù A and Adibi A 2020 *Nanophotonics* **9** 1189
[27] Tonkaev P, Sinev I S, Rybin M V, Makarov S V and Kivshar Y 2022 *Chemical Reviews* **122** 15414
[28] Delaney M, Zeimpekis I, Lawson D, Hewak D W and Muskens O L 2020 *Adv. Funct. Mater.* **30** 2002447
[29] Delaney M, Zeimpekis I, Du H, Yan X, Banakar M, Thomson D J, Hewak D W and Muskens O L 2021 *Sci. Adv.* **7** eabg350
[30] Palik E D 1985 *Handbook of optical constants of solids* (Orlando: Academic Press) pp. 547–569
[31] Abbas M A, Zubair A, Riaz K, Huang W, Teng J, Mehmood M Q and Zubair M 2020 *Opt. Express* **28** 23509
[32] Overvig A C, Malek S C, Carter M J, Shrestha S and Yu N 2020 *Phys. Rev. B* **102** 035434
[33] Bulgakov E N and Maksimov D N 2017 *Phys. Rev. Lett.* **118** 267401
[34] Jin J, Yin X, Ni L, Soljačić M, Zhen B and Peng C 2019 *Nature* **574** 501
[35] Kang M, Zhang S, Xiao M and Xu H 2021 *Phys. Rev. Lett.* **126** 117402
[36] Yuan L and Lu Y Y 2018 *Phys. Rev. A* **97** 043828
[37] Mackay A 1989 *Electron. Lett.* **25** 1624
[38] Ndao A, Hsu L, Cai W, Ha J, Park J, Contractor R, Lo Y and Kanté B 2020 *Nanophotonics* **9** 1081
[39] Su W, Chen X, Geng Z, Luo Y and Chen B 2020 *Results in Physics* **18** 103340
[40] Hsiao H H, Hsu Y C, Liu, A Y, Hsieh J C and Lin Y H 2022 *Adv. Opt. Mater.* **10** 2200812
[41] Watanabe K and Iwanaga M 2023 *Nanophotonics* **12** 99
[42] Li H, Xing J, Shi Y, Yu S and Zhao T 2023 *Opt. & Laser Technol.* **157** 108752